Pharmacological Research 221 (2025) 107982

Contents lists available at ScienceDirect

Pharmacological Research

journal homepage: www.elsevier.com/locate/yphrs

# Nanotoxin induces *in situ* pyroptosis to sensitize αPD1 to ablate metastases in microsattellite stable colorectal cancer

Luis M. Carrasco-Díaz [a,b,c], Marc Otero-Mateo [a], Patricia Álamo [a,b,c], Alberto Gallardo [d], Anna C. Virgili [a,e], David Páez [e,f], Eric Voltà-Durán [c,g], Antonio Villaverde [c,g,h], Esther Vázquez [c,g,h], Ugutz Unzueta [a,b,c,h], Isolda Casanova [a,b,c], Lorena Alba-Castellon [a,b,c,*], Ramon Mangues [a,b,c,*]

[a] *Institut de Recerca Sant Pau (IR SANT PAU), Sant Quintí 77-79, Barcelona 08041, Spain*
[b] *Josep Carreras Leukaemia Research Institute (IJC Sant Pau), Barcelona, Spain*
[c] *CIBER de Bioingeniería, Biomateriales y Nanomedicina (CIBER-BBN), Spain*
[d] *Department of Pathology, Hospital de la Santa Creu i Sant Pau, Barcelona 08041, Spain*
[e] *Department of Medical Oncology, Hospital de la Santa Creu i Sant Pau, Barcelona 08041, Spain*
[f] *CIBER de Enfermedades Raras (CIBERER), Spain*
[g] *Institut de Biotecnologia i de Biomedicina, Universitat Autònoma de Barcelona, Bellaterra 08193, Spain*
[h] *Departament de Genètica i de Microbiologia, Universitat Autònoma de Barcelona, Bellaterra 08193, Spain*

ARTICLE INFO

*Keywords:*
Targeted nanotoxin
In situ release
Pyroptosis
T cell recruitment
Antimetastatic effect
Immuno-oncology

ABSTRACT

Nanomedicine has not generated anticancer immunotherapies because of insufficient targeted specificity, lack of immunity, and associated toxicity. We developed a T22-DITOX-H6 (TDX) nanotoxin to selectively release the diphtheria toxin in the cancer cells in immunosuppressed CXCR4-overexpressing (CXCR4 +) colorectal (CRC) models, inducing pyroptosis and anticancer effect.

Microsatellite stable (MSS) CRC patients do not respond to current immunotherapy. Since pyroptosis is highly immunogenic, we treated with TDX immunocompetent CXCR4 + CT26 MSS metastatic CRC models to selectively deliver the toxin to induce in situ pyroptosis mediated by the activation of NLRP3, Caspase-1 GSDMD and IL-1β. In contrast to immunosuppressed, in situ pyroptosis by TDX in immunocompetent models trigger CD8 + T cell recruitment, activation and killing of cancer cells in tissues, mimicking the pyroptosis that the host induces to kill diphtheria-infected cells.

The combination of TDX and αPD1 further increases CD8 + recruitment and perforin secretion, achieving a tissue-specific antimetastatic activity in mesentery, peritoneum, and lung, and especially in liver metastases, without systemic toxicity. This is the first time that a novel nanomedicine achieves local T cell activation and antimetastatic effect mediated by pyroptosis and immunogenic cell death, whereas the combination with αPD1 enhances T cell activation, reaching a synergistic response in MSS CRC models.

## 1. Introduction

Nanomedicine has not generated anticancer immunotherapies so far. This is most likely because of insufficient targeted specificity, inability to engage the system, and associated toxicity [1,2] We previously found that apoptosis is the main cell death activated in CXCR4-overexpressing (CXCR4 +) immunosuppressed cancer models when treated with nan-transporters (e.g. T22-GFP-H6) chemically bound to small drugs (Flox-uridine, Ara-C or Auristatin) [3–5]. However, apoptosis is unable to activate the immune system against the tumors because it is non-immunogenic [6].

In contrast, we consistently demonstrate the nanotoxin T22-DITOX-H6 (TDX) induces pyroptosis in immunosuppressed CXCR4 + cancer models, which is a highly immunogenic cell death [6]. Thus, once the TDX delivers the *Corynobacterium diphtheria* toxin in target cancer cells, it triggers selective caspase and GSDMD-mediated pyroptosis to block tumor growth and metastases, without systemic toxicity, in CRC and head and neck cancer (HNSCC) models [7–11].

* Corresponding authors at: Institut de Recerca Sant Pau (IR SANT PAU), Sant Quintí 77-79, Barcelona 0841, Spain.
*E-mail addresses:* lalba@santpau.cat (L. Alba-Castellon), rmangues@santpau.cat (R. Mangues).

https://doi.org/10.1016/j.phrs.2025.107982
Received 22 July 2025; Received in revised form 26 September 2025; Accepted 6 October 2025
Available online 11 October 2025

TDX is a modular nanoparticle built by monomers. Each monomer is composed of a T22 peptide in the N-term that acts as a ligand for the CXCR4 receptor, followed by the catalytic domain and the translocation domain of the *Corynebacterium diphtheriae* toxin, whereas in the C-term a 6-His tail maintains the nanoparticle structure [7]. The multiple ligands confer selective endocytosis in CXCR4 + cancer cells to release the toxin, by furin cleavage, to inhibit eEF2 to block protein synthesis to kill cancer cells ( [8–10]), which induces ribotoxic stress to induce pyroptosis [12].

On this basis, we aimed to treat with TDX a novel immunocompetent CXCR4 + metastatic CT26 CRC (mCRC) microsatellite stable (MSS) mouse model, which derives from the cell line proven to be MSS, with proficient DNA mismatch repair and low tumor mutational burden [13–15] to obtained a response. Thus, we expect the TDX to induce pyroptosis to recruit and activate T cells to overcome the resistance to ICIs in CRC MSS mouse models.

Therefore, we look to achieve *in situ* release of the toxin in metastatic and tumor tissues to induce the activation of NLRP3, Caspase-1, GSDMD and IL-1β, mediated pyroptosis in this novel model to achieve T cell recruitment and activation to trigger an antimetastatic effect since this cell death is highly inflammatory [16] and the most immunogenic of cell death types [6], We also expected that the combination of TDX will sensitize to αPD1 (anti-PD1) because of the inflammation induce by pyroptosis will enhance the antimetastatic effect.

This approach is supported by the fact that 85 % of patients with metastatic MSS CRC do not respond to immune checkpoint inhibitors (ICIs), such as αPD1 [15,17]; being, therefore, a relevant unmet medical need. We found that TDX induces pyroptosis in CXCR4 + metastases and tumor tissues to generate local inflammation, cytokine secretion, and T cell recruitment in CXCR4 + liver, lung, mesenteric, and peritoneal metastases and tumors. Moreover, the TDX + αPD1 activation and a synergistic antimetastatic effect, which eliminated liver metastases, without inducing systemic toxicity. Therefore, the *in situ* pyroptosis induced by TDX to recruit and activate cytotoxic T cells at the different metastatic sites and tumors, and a synergistic effect by TDX+ αPD1 combination, without systemic toxicity. This opens a novel immunotherapy approach based on bacterial toxins that may have an impact in future immunotherapy.

## 2. Materials and methods

### 2.1. Nanotoxin

T22-DITOX-H6 (TDX) nanoparticle production, purification and characterization have been previously described [7]. Cell disruption was performed in an EmulsiFlex-C5 system (Avestin, Ottawa, Canada) by 3 rounds at 8000 psi and proteins were purified using a HisTrap HP Column (GE Healthcare, Chicago, USA) in ÄKTA pure system (GE Healthcare, Chicago, USA). The oligomeric protein nanoparticle size was determined by Dynamic Light Scattering (DLS) in a Zetasizer Pro (Malvern Instruments, Malvern, United Kingdom) reaching a diameter of around 100 nm.

### 2.2. Cell lines and cell culture

The CRC cell line CT26 was purchased from ATCC (CRL-2638) (Manassas, USA). CT26 (CT26-Par) was transduced with a mouse CXCR4 plasmid (pLV-EF1A-Puro-mCXCR4, VectorBuilder Chicago, USA) to generate the CT26.mCXCR4 + cell line as previously described [10]. We also generated CT26.LMet2 cells derived from the CT26.mCXCR4 + cell line by three in vivo passages of an intrasplenic model to generate liver metastases. The protocol to generate this cell line is explained in the supplementary materials.

CT26.mCXCR4 + and CT26.LMet2 cell lines were cultured in medium Roswell Park Memorial Institute (RPMI) 1640 (Gibco, Life Technologies, Waltham, USA) supplemented with 10 % Fetal Bovine Serum (FBS), 100 U/mL penicillin/streptomycin, and 2 mM glutamine (Gibco, Life Technologies, Waltham, USA) and incubated at 37 ºC and 5 % $CO_2$ in a humidified atmosphere.

The Western blot of CT26.mCXCR4 + cells exposed to TDX determined their expression with antibodies of Caspase-1 (Cell Signaling, 83383) and Caspase-1 p20 (Invitrogen, PA599390) and also of Gasdermin-D (Novus Biologicals, NBP2–33422) and CL-GSDMD (Cell Signaling, 10137) and H3 as protein control (Cell Signaling 9718).

### 2.3. In vivo experiments

BALB/c mice were obtained from Charles River Laboratories (Wilmington, USA). Mice were housed in a specific pathogen-free (SPF) environment with sterile food and water ad libitum. All procedures were previously approved by the institutional Hospital de la Santa Creu i Sant Pau Animal Ethics Committee and the Catalonian Government, protocol nº 12001. To generate the subcutaneous colorectal (CRC) model, mice were implanted in the subcutis with $2.5 \times 10^5$ CT26.mCXCR4 + cells. In the orthotopic model, mice were implanted with $10^4$ CT26.LMet2 cells in 50 µL (1:1) (RPMI 1640:Matrigel (Corning, ThermoFisher Scientific, Waltham, USA)) in the cecum as previously described [18]. In both experiments, at day 9 post-injection mice-bearing tumors were randomized in four groups (TDX, αPD-1, TDX+αPD1 combination, and Vehicle). TDX mice were intravenously (i.v.) administered with doses of 0.5 mg/kg of TDX dissolved in 100 µL of Vehicle (166 mM $NaCO_3H$ pH8), three times per week (t.i.w) x6 doses. Mice in the αPD-1 group were intraperitoneal (i.p.) treated with 10 mg/kg of anti-PD-1 (αPD1, #BE0146 BioXCell) dissolved in 100uL of buffer (22 mM $Na_2HPO_4$, 9.9 mM $NaH_2PO_4$, 136 mM NaCl, pH7), two times a week (b.i.w.) x 4 doses. Mice from the TDX+ αPD1 combination group that received sequential and repeated doses. Thus, this group was administered i.v with 0.5 mg/kg of TDX, 3 t.i.w. x 6 doses, and i.p. with 10 mg/kg of αPD-1 b.i.w. x 4 doses. Finally, mice of the Vehicle group were administered intravenously (i.v.) with 100 µL of TDX's buffer, t.i.w. x6 doses and i.p. with 100 µL of αPD1's buffer, b.i.w. x4 doses.

Animal body weight was registered three times per week, whereas subcutaneous tumor size was measured with a caliper (tumor volume= $width^2$ x length/2) every TDX administration during the time course of the experiment, and their volume ex vivo at the end of the experiment.

Mice were euthanized 72 h after the last dose of the TDX. Then, tumors and organs were collected for further histopathological analysis. Blood was extracted by intracardiac puncture, for blood tests, including white blood cells, red blood cells, and further liver and kidney function analysis and placed in EDTA-tubes and centrifuged at 21,000 g for 10 min at 4 ºC, plasma was store at - 80 ºC.

### 2.4. Sample processing for hematoxylin and eosin (H&E), DAPI and immunohistochemical (IHC) staining to evaluate the molecular and cellular changes in tissues

Paraffin-embedded organs were cut in 4 µm sections for staining. Organ sections were stained with H&E and analyzed by two independent observers. In the orthotopic model, we distinguished micro- and macrometastases measuring their area in sections of the affected organs (liver (LV), lung (LG), mesentery (MS) and peritoneum (PRT)). Macrometastases had an area > 785,000 $\mu m^2$, while micrometastases had an area lower than this threshold as established by Folkman [19].

IHC staining was performed in a DAKO Autostainer Link48 (Agilent Technologies, Santa Clara, USA) following the manufacturer's instructions. Firstly, sections were dewaxed, the antigen retrieval was made using PTLink (DAKO) and finally stained in DAKO Autostainer Link48 using the following primary antibodies: NLRP3 (abcam ab2770449), IL-1β (Abcam ab205924) cleaved Caspase-1 p20 (CL Casp-1) (1:400, Invitrogen, ThermoFisher Scientific, Waltham, USA. Retrieval pH low, DAKO), IFNγ (1:200, Invitrogen, ThermoFisher Scientific, Waltham, USA. Retieval pH high, DAKO), CD8 + (1:500, Cell Signaling Technologies, Danvers, USA. Retrieval pH Low, DAKO), Perforin (1:400,

Abcam, Cambridge, UK. Retrieval pH high). IHC positive staining was identified and quantified with the SlideViewer software (3DHistech, Budapest, Hungary). In tissue section of tumors or metastases affected organs (LV, LG, MS, PRT), we determine CD8 + T cell infiltration measuring the total stained- positive cells per $mm^2$, while CL Casp-1, IFNγ and perforin secretion were assessed as total stained-positive pixels per $mm^2$.

DAPI staining was performed as follows, paraffin-embedded sections were dewaxed, rehydrated, and permeabilized with 0.5 % Triton X-100. Then, sections were stained with DAPI mounting medium (ProLong™ Gold Antifade Mountant, Thermo Fisher Scientific, Waltham, USA) and incubated at 4ºC overnight. Cell death quantification was performed by counting the number of condensed nuclei per $mm^2$.

### 2.5. Plasma and blood analysis

To assess the possible systemic toxicity associated to TDX treatment or its combination with αPD1 in the CT26. mCXCR4 + immunocompetent mice in the red and while blood cell lineages, the blood from the mice was analyzed using the Mindray BC-5000 Vet hematology analyzer.

In order to evaluate the possible toxicity in the liver and kidney, we measured the hepatic function by aspartate transaminase (AST) and alanine transaminase (ALT) enzyme activities, renal function by creatinine and uric acid and albumin, that were measured in plasma samples with commercial kits (Roche Diagnostics, Basel, Switzerland) adapted for a COBAS 6000 autoanalyzer (Roche Diagnostics, Basel, Switzerland).

### 2.6. Cell viability assays

Cell Proliferation Kit II (XTT) (Roche Diagnostics, Basel, Switzerland) was used according to the manufacturer's instructions. Cells were seeded in 96-well plates (5,000 cells/well) and treated with either T22-DITOX-H6 or vehicle for 48 h. XTT reagent was added and measured at 492 nm (FLUOstar OPTIMA spectrophotometer (BMG Labtech, Ortenberg, Germany)) after 4 h of incubation at 37º C.

### 2.7. Western blot

In order to obtain cell extracts, CT26-LMet2 cells were seeded in petri dish (Sigma-Aldrich, Burlington, USA) and treated with either vehicle or 10 nM of T22-DITOX-H6 for 24 h. After incubation time, cells were washed twice with cold PBS and resuspended in SDS lysis buffer (0.05 M Tris-HCl pH 6.8, 2 % SDS, 10 % glycerol). Cells were lysed passing the cell suspension trough a 27-G syringe ten times, and then the suspension was centrifuged for 10 min at 21,000 g at 4ºC. Whole cell proteins extracts were quantified (BCA Gold Protein Quantification kit (Thermo Fisher Scientific, Waltham, USA)) and 40 μg of proteins were used for SDS-PAGE electrophoresis. Proteins were transferred to a nitrocellulose blotting membrane (GE Healthcare Life Sciences, Chicago, USA), blocked with 5 % skim milk in TSB-T for 1 h at room temperature, and incubated overnight at 4ºC with the primary antibodies: anti-mouse cleaved GSDMD (1:1000, Cell Signaling Technologies, Danvers, USA), full GSDMD (1:1000, Novus Biologicals, Colorado, USA), cleaved caspase-1 (1:1000, Invitrogen, ThermoFisher Scientific, Waltham, USA), full caspase-1 (1:1000, Cell Signaling Technologies, Davers, USA), and Histone 3 (1:5000, Cell Signaling Technologies, Danvers, USA). Afterwards, membranes were washed with TBS (Biorad, Hercules, USA) -Tween 20 (1:1000) (Sigma-Aldrich, Burlington, USA) and incubated 1 h at RT with a HRP-conjugate secondary antibody (1:10000, Jackson Immune Research, Philadelphia, USA), washed with TBS-T and visualized with SuperSignal West Pico Chemiluminiscent Substrate using the ChemiDoc XRS+ imaging system (Biorad, Hercules, USA). Densitometry analysis was performed using imageJ software.

### 2.8. Statistical analyses

Data are presented as mean ± Standard Error of the Mean (SEM). Statistical analyses were performed using GraphPad Prism 8 software (GraphPad Software, San Diego, USA). For in vivo experiments, comparisons between two groups were performed using the Mann–Whitney test. For in vitro experiments, comparisons between two groups were analyzed with the unpaired Student's *t*-test, and comparisons involving more than two groups were analyzed using one-way ANOVA. Differences were considered statistically significant when $p < 0.05$. All experiments were performed at least in triplicates.

## 3. Results

### 3.1. TDX induces 'in situ' pyroptosis and local CD8 T cell recruitment in targeted tumor tissues, whereas its combination with αPD1 increases its effectiveness

Based on the pyroptosis triggered by the TDX nanotoxin that lead to the inhibition of subcutaneous (SC) tumor growth and metastatic dissemination in immunosuppressed CXCR4 + CRC mouse models [8,10,11], we tested, in a syngeneic immunocompetent SC CXCR4 + CT26 MSS CRC (scCRC), the TDX capacity to induce tumor pyroptosis and T cell recruitment and activation in cancer target tissues. In addition, we tested if the TDX+ αPD1 combination achieves a synergistic antitumor effect in this model. We compared the antitumor effect in four mouse groups, treated with TDX (n = 9), αPD1(n = 8), TDX+ αPD1 (n = 6), or Vehicle (n = 7) according to the sequential dose regime (Fig. 1a) described in detail in materials and methods.

Both single TDX or single αPD1-treated mice inhibit tumor growth during the tested period, as compared to Vehicle; nevertheless, they maintained positive tumor growth in the 67 % of mice in TDX-treated and 63 % in the αPD1 group of mice (Fig. 1b). In contrast, the sequential TDX+ αPD1 triggered a higher tumor growth blockade, reaching regression or tumor stabilization in a majority of mice (83 %), recording tumor volumes close to zero, except for one animal (Fig. 1b), thus achieving a synergistic antitumor effect.

Moreover, at the end of the experiment, we observed that all three treatment groups TDX, αPD1 and TDX+ αPD1, significantly reduced the ex vivo SC tumor volume, as compared to Vehicle, showing the TDX+ αPD1 the most significant reduction (Fig. 1c). This result is consistent with the higher number of cell death events per $mm^2$ in the TDX group. In contrast, the tumor that continued to grow in the combination group did not show any significant differences in cell death compared to the Vehicle group, suggesting a lack of response to therapy in this particular tumor. (Fig. 1d)

Next, we studied the cellular and molecular changes in SC tumor tissues associated to tumor growth control by TDX, especially focusing on T cell activation. However, we were not able to perform this study on αPD1 or combination-treated mice because of the lack of available tissue. The tested hypothesis was that TDX will trigger pyroptosis to inflame and recruit T cells in tumor tissue in this immunocompetent MSS CRC model, trying to mimic the pyroptosis induced by the diphtheria exotoxin in epithelial infected cell, in which the host respond by T cell recruiting and activation to fight the infection [12,16,20], considering that pyroptosis activates the adaptive immune system to induce immunogenic cell death (ICD) [6,21].

Consistently, TDX induced pyroptosis, showing a significant increase in NLRP3, active cleaved Caspase-1 p20 and IL-1β and two-fold higher cell dead number in tumors than in Vehicle-treated (Fig. 1e). Interestingly, TDX-induced pyroptosis triggered secretion of IL-1β asnd INFγ in tumor tissue, and a 4-fold increase in CD8 + T cell and Perforin vesicle degranulation densities (Fig. 1e), all signs of T cell activation and ICD, as compared to Vehicle-treated mice. Therefore, the observation of the TDX capacity of inducing T cell recruitment and T cell activation in an MSS SC CRC tumors was exciting, considering that MSS CRC patients are

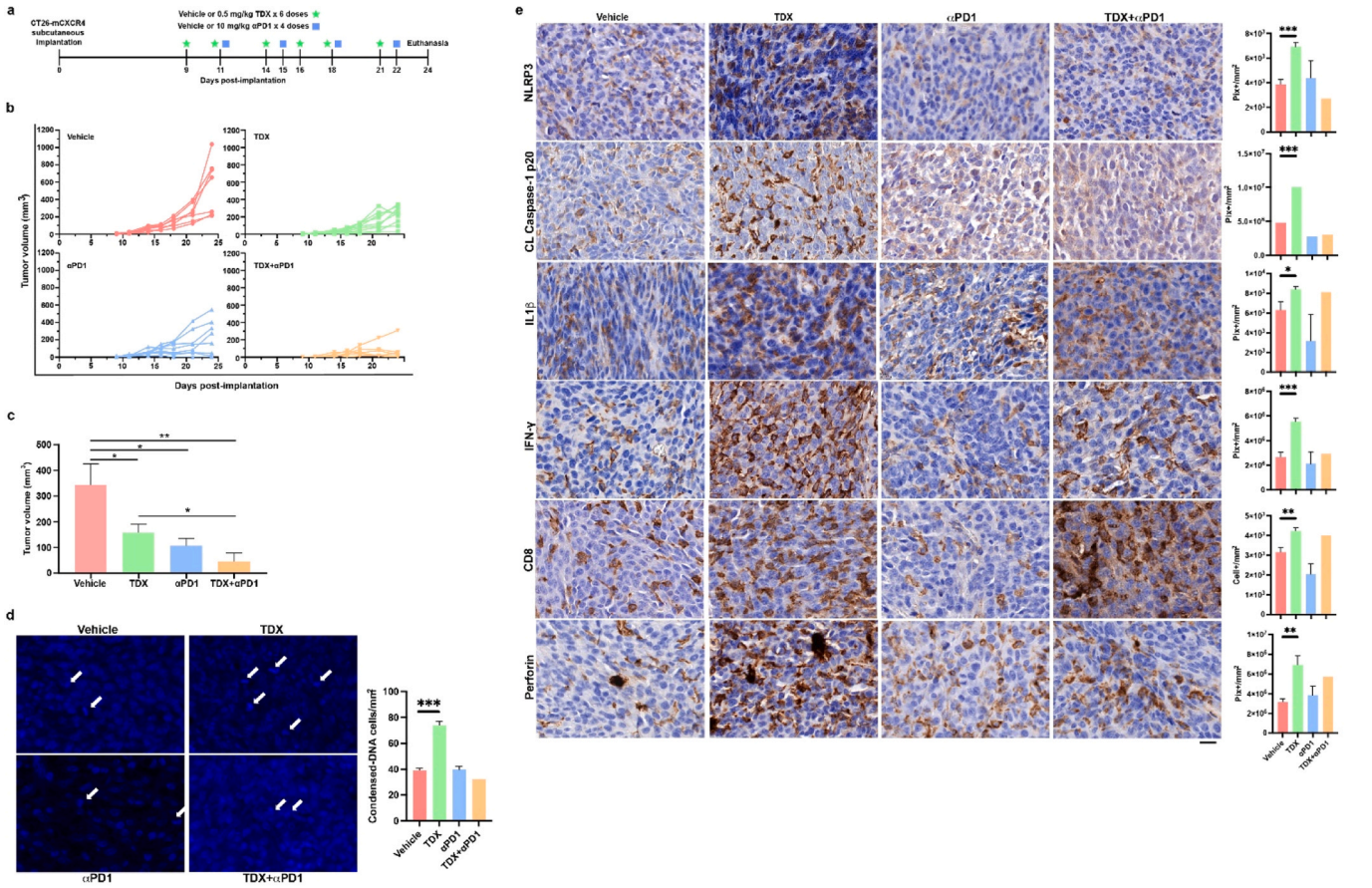


**Fig. 1.** TDX induces pyroptosis mediated by NLRP3, CL-Caspase-1, IL-1β, IFNγ secretion, T cell infiltration and activation in the syngeneic MSS scCRC model derived from the CT26.mCXCR4, whereas its combination with αPD1 triggers tumor blockade (a) Schematic representation of the experimental and dosage timeline. (b) Evolution of individual tumor volumes throughout the experiment. (c) Final tumor volume measured ex vivo at the experiment's end point. (d) Representative images of tumor sections stained with DAPI to detect condensed DNA. Quantitation of tumor cells with condensed DNA per $mm^2$. Scale bars = 20 μm. (e) Representative tumor sections from mice treated with TDX or Vehicle, stained by immunohistochemistry (IHC) for NLRP3, CL caspase-1 p20, IL-1β, IFNγ, CD8 to measure T cell infiltration and perforin secretion, to measure T cell activation. Scale bars = 20 μm. Quantitation of positive stained pixels (CL caspase-1, IFNγ, perforin) or cells (CD8) per $mm^2$. Error bars indicate ±SEM. * $p < 0.05$; ** $p < 0.01$; **** $p < 0.0001$. MSS: microsatellite stable. CRC: colorectal cancer.

resistant to immunotherapy due to immune exclusion [22]. On the other hand, the results of a higher tumor growth inhibition by the TDX+ αPD1 than the single drugs or Vehicle suggest a synergistic effect between TDX and the checkpoint inhibitor αPD1. In summary, TDX, as single drug, induces T cell infiltration and activation, whereas the TDX+ αPD1 combination triggers tumor blockade in a syngeneic subcutaneous CXCR4 + MSS CRC model. These findings encouraged us to test the effect of the combination in an orthotopic MSS metastatic colorectal cancer (mCRC) model.

### 3.2. *TDX induces in situ pyroptosis and local CD8 T cell recruitment in targeted metastatic tissues*

First, we generated a novel orthotopic MSS metastatic CXCR+ LMet2 CT26 model (ORT MSS model) following the protocol described in Supplementary Material and Methods to generate the CT26.LMet2 metastatic cells, which we confirmed high mCXCR4 overexpression in the membrane (Supplemental Fig. 1a, b).

We selected the orthotopic MSS metastatic CXCR+model derived from the LMet2 CT26 cells, rather the metastatic orthotopic model derived from the CT26.mCXCR4, because it showed a higher metastatic burden. Moreover, we compared the sensitivity to TDX for he CT26. mCXCR4 + CRC cells and the CXCR4 + LMet2 CRC cell line to demonstrated that both has a similar cytotoxicity (Supplemental Fig. 1 c). Moreover, the Western blot of CT26.mCXCR4 + cells exposed to TDX to assess demonstrated the induction of pyroptosis mediated by the activation of Caspase-1 and of Gasdermin-D (GSDMD) cleavage (Supplemental Fig. 1d). Therefore, the mCRC orthotopic model was developed by implanting CT26.LMet2 in the mouse cecum, which develops metastases in the most relevant organs in CRC; liver (LV-Mets), lung (LG-Mets), mesentery (MS-Mets), and peritoneum (PRT-Mets). Thus, nine days after CT26.LMet2 orthotopic implantation, all mice had a grown primary tumor of around 0.4 g (Supplemental Fig. 2a), while 40 % of the mice presented, at least, one metastatic focus in the liver (Supplemental Fig. 2b,c).

Next, we run a new experiment to test the antimetastatic effect of TDX, as a single drug, and study markers of pyroptosis and immune activation. To that purpose, at day nine after cell implantation, we randomized mice with CT26.LMet2 in two groups (TDX and Vehicle) applied the following dosage: TDX (n = 8) were i.v. administered with 0.5 mg/kg, t.i.w. x6 doses, whereas the Vehicle group (n = 10) was i.v. injected with the TDX's Vehicle, t.i.w. x6 doses (Fig. 2a). At the end of the experiment, we observed a half reduction in the number of metastatic foci induced in TDX mice in liver (LV-Mets), lung (LG-Mets), mesentery (MS-Mets) and peritoneum (PRT-Mets) as compared to Vehicle-treated mice (Fig. 2b).

Next, we studied markers of pyroptosis and T cell activation after TDX treatment only in the primary tumor of the ORT CRC model, measuring the intensity of CL Caspase-1, as marker of pyroptosis, as described [9] and infiltration of cytotoxic T cells in tumor, measuring

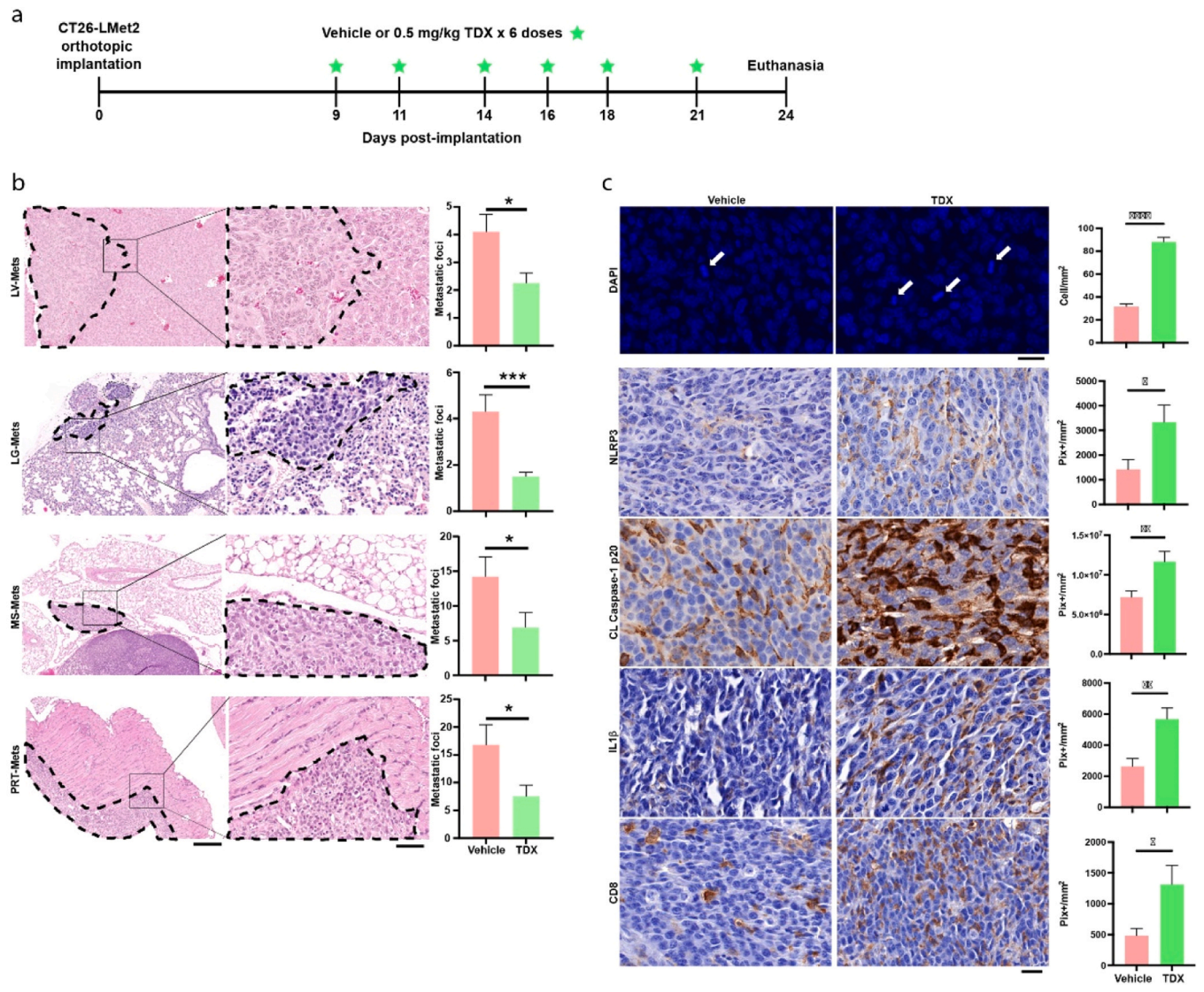


**Fig. 2.** TDX, as a single drug, induces pyroptosis and T cell activation in primary tumor and an antimetastatic effectin LV-Mets, LG-Mets, MS-Mets and PRT-Mets in an MSS ORT derived from the LMet2 CT26 CXCR4$^+$ CRC model. (a) Schematic representation of the experimental and dosage timeline and representative images of the H&E histology of the primary tumors for the vehicle- and TDX-treated groups. (b) H&E-stained sections of organs showing representative metastatic foci in the liver (LV-Mets), lung (LG-Mets), mesentery (MS-Mets) and peritoneum (PRT-Mets) and quantitation of total metastatic foci per section. Scale bars = 200 μm and 50 μm (zoom-in view). (c) Representative sections of primary tumors stained with DAPI (blue) to detect condensed DNA, indicative of dead cells, and quantitation of tumor cells with condensed DNA per mm$^2$ of mouse tumor sections treated with TDX or Vehicle followed by representative tumor sections treated with TDX or Vehicle, stained by immunohistochemistry (IHC) for NLPP3, CL caspase-1 p20, IL-1β and infiltrated cytotoxic CD8 + T cells. . Quantitation of stained positive pixels (CL casp-1) or cells (CD8) per mm$^2$. Scale bars = 20 μm. Error bars indicate ±SEM. * $p < 0.05$; *** $p < 0.001$; **** $p < 0.0001$.

CD8 + T cells density in the occupied tissue area. We observed a two-fold increase in DNA condensation and the activation of NLRP3, CL Caspase-1 and IL1β, and also a three-fold increase in CD8 + density in the primary tumor in TDX compared to Vehicle-treated mice (Fig. 2c). This is a relevant finding confirming that the activation of pyroptosis by TDX induces T cell recruitment in the primary tumor of the MSS CRC cancer model, a finding similar to that observed in the MSS SC tumor model (Fig. 1e) and supporting TDX capacity to induce the recruitment of T cells to tumor tissues.

Once we demonstrated that TDX as single drug activates T cells triggered by pyroptosis induction, we next evaluated the antitumor and antimetastatic response to treatment by TDX, αPD1 or TDX+ αPD1 combination using the MSS ORT mCRC model and their association in the molecular and cellular immune changes induced in primary tumor and metastatic tissues at all sites.

### *3.3. Sequential TDX+ αPD1 combination induces cancer cell killing associated with CD8 T cell activation and IFNγ and Perforin secretion*

First, we studied the antitumor effect of single drugs and the TDX+ αPD1 combination using the orthotopic metastatic CRC model derived from the CT26.LMet2 cell, as above. Nine days after cell implantatin, mice were randomized in 4 groups. TDX-treated mice (n = 7) were i.v. injected with 0.5 mg/kg TDX, t.i.w. x6 doses; the αPD-1 group (n = 6) was i.p. treated with 10 mg/kg of αPD1, b.i.w. x4 doses; the TDX+ αPD1 group (n = 7) was administered i.v. with 0.5 mg/kg of TDX, t.i.w. x6 doses, and i.p. with 10 mg/kg of αPD-1 b.i.w. x4 doses; and finally, the Vehicle group (n = 8) was i.v. administered with the buffer of TDX, t.i.w. x6 doses and i.p. injected the buffer of αPD1, b.i.w. x4 doses (Fig. 3a).

The primary tumor response to the combination therapy shows a significant and synergistic reduction in tumor weight, as compared to TDX or αPD1 or Vehicle (Fig. 3b). Moreover, in primary tumor tissue

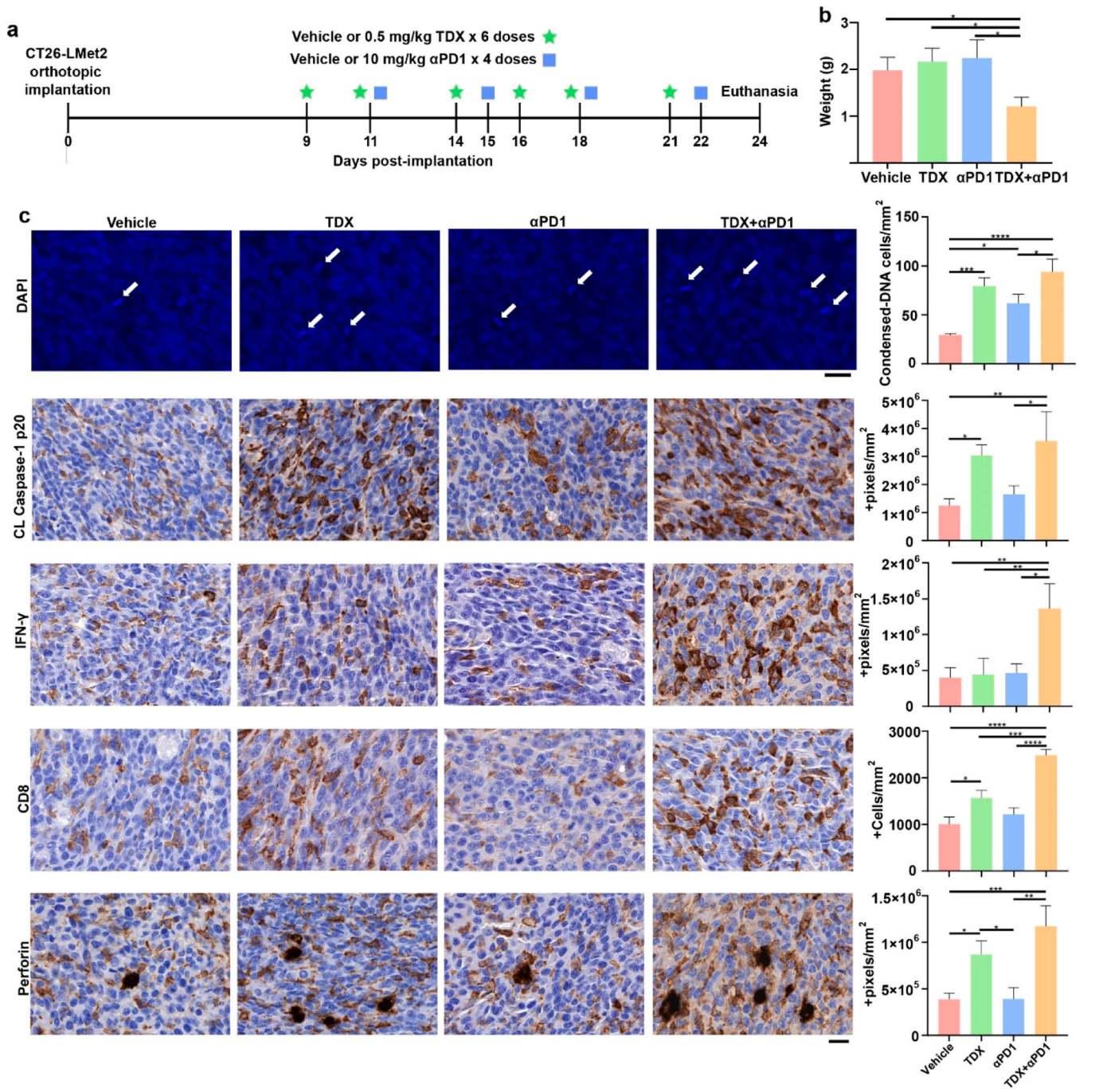


**Fig. 3.** TDX+ αPD1 combination inhibits primary tumor growth associated with Interferon γ secretion, T cell ativation and perforin degranulation in the orthotopic (ORT) derived from the LMet2 MSS mCRC model. (a) Graphical depiction of the experimental and dosage timeline. (b) Final tumor weight measured ex vivo at the experiment's endpoint. (c) Samples images of tumor sections from every experimental group stained with DAPI to detect condensed DNA. Quantitation of tumor cells with condensed DNA per $mm^2$ (Scale bars = 20 μm) and illustrative images of tumor sections from mice treated with Vehicle, TDX, αPD1 or, TDX+ αPD1, stained by IHC for CL casp-1, IFNγ (e), CD8 and perforin). Evaluation of positive stained pixels (CL caspase-1, IFNγ, perforin) or cells (CD8) per $mm^2$. Scale bars = 20 μm. Error bars indicate ±SEM. * $p < 0.05$; ** $p < 0.01$; *** $p < 0.001$; **** $p < 0.0001$.

there is an increase in condensed DNA, and in CL Caspase-1 in both, the TDX and TDX+ αPD1 groups, but not in αPD1 group which supports the induction of pyroptosis exclusive by TDX in primary tumor (Fig. 3c). Pyroptosis was followed by an increase in IFNγ levels only in combination-treated mice, as compared to TDX, αPD1 or Vehicle groups. In addition, the combination treated primary tumor displays higher densities of CD8 + T cell and increase in perforin secretion compared to the rest of the groups (Fig. 3c). The reason to test the levels of the pro-inflammatory cytokine IFNγ, was based on the reports of IFNγ activation triggering ICD, an event mediated by the recruitment of cytotoxic CD8 + T cells in CRC [23,24] and the association between an IFNγ signature and good prognosis in CRC patients [25]. Moreover, we measured perforin secretion to determine if the infiltrated T cells in tumor tissue could induce ICD in target cancer cells, since this is mediated by the release of perforin cytotoxic granules once the immune synapse is established [26].

In summary, TDX+ αPD1 combination therapy inhibits primary tumor growth by increasing Interferonγ secretion, T cell infiltration and

perforin degranulation in the orthotopic (ORT) MSS mCRC model.

### 3.4. TDX+ αPD1 induces antimetastatic in MSS mesentery and peritoneum associated with CD8 T cell activation and IFNγ secretion

We here describe the antimetastatic effect of single drugs and the TDX+ αPD1 combination dosage described in 3 (Fig. 3a), within the same experiment using the MSS CXCR4 + CT26 mCRC model, and focusing in the observed response to treatment in the mesenteric (MS-Mets) and peritoneal (PRT-Mets) metastases and the associated molecular and cellular immune changes in these tissues.

We found TDX+ αPD1 to exert a significant synergistic antimetastatic effect in MS-Mets by reducing three-fold the metastatic foci number and area, compared to TDX, αPD1 or Vehicle; nevertheless, despite the significant response induced by the combination, it did not achieve their elimination, since all mice bear MS-Mets at the end of the experiment (Fig. 4a). On the other hand, the TDX induced pyroptosis in MS-Mets tissues, mediated by CL Casp-1, at a level similar to the TDX+ αPD1- treated mice (Fig. 4b). Moreover, the TDX+ αPD1 combination increased significantly the Interferon γ levels, as compared to αPD1 or Vehicle, being these levels similar to those found in TDX-treated mice. These effects were associated with a huge increase of CD8 + density in MS-Mets in the combination that was higher than in TDX-treated mice, whereas the αPD1 did not increase since it was similar to the levels observed in the Vehicle (Fig. 4b). In addition, we observed an increase in perforin degranulation in the TDX group. However, surprisingly, the perforin levels in the combination did not differ from single drugs or the Vehicle (Fig. 4b).

In PRT-Mets (Fig. 4c) the combination exerted a significant synergistic antimetastatic effect by reducing their metastatic foci area (Fig. 4c) but did not achieve the ablation of metastases at this site since all mice bear PRT-Mets at the experiment end. The TDX group showed the more potent pyroptosis measured as CL Casp-1 expression, whereas the combination also induced pyroptosis, reaching a level similar to the TDX group. Finally, both, the combination and the TDX group increased the level of Interferonγ and CD8 + T cell density in PRT-Mets tissues, as compared to αPD1 or vehicle, and again, surprisingly, perforin degranulation did not increase in the combination, TDX and αPD1, since their levels were similar to those measured in Vehicle-treated mice (Fig. 4d). In summary, TDX+

αPD1 combination therapy significantly reduces the metastatic burden in the mesentery and peritoneum in the orthotopic model (ORT MSS model).

### 3.5. TDX + αPD1 induces a synergistic effect in MSS liver and lung metastases, whereas the liver effect associates with CD8 T cell activation and Perforin secretion

In this section, we describe the antimetastatic effect of single drugs and the sequential TDX+ αPD1 combination, within the same experiment and dosage described in 3 (Fig. 3a) using the MSS CXCR4 + CT26 mCRC model. Here, we focus on the LV-Mets and LG-Mets response to TDX+ αPD, TDX or αPD1 and their molecular and cellular immune changes in their tissues. We found that TDX+ αPD1 therapy obtains a dramatic antimetastatic effect in LV-Mets that achieves their elimination. Thus, 86 % of the mice were metastases-free in LV-Mets at the end of the experiment (Fig. 5a). Moreover, in the TDX+ αPD1-treated group all mice were free of micro- and macrometastases in the liver, except for a mouse that bears only one macrometastases (Fig. 5b).

In contrast, Vehicle, TDX or αPD1-treated mice bear all micrometastases (area <785,000 $\mu m^2$) and macro-mestastases (area >785000 $\mu m^2$) thus, none of the mice of these groups were metastases free (Fig. 5b).

On the other hand, mice administered with TDX or αPD1 reduce their metastases number, as compared to Vehicle. However, the mice of these three groups do not become metastases-free (Fig. 5c). Interestingly, the 14 % of mice that are not eliminated by TDX+ αPD1 therapy (thus, bearing still LV-Mets) achieve a high reduction of foci number as compared to TDX or αPD1, which, in turn, these two groups induce a significantly higher antimetastatic effect compared to the vehicle-treated group (Fig. 5c).

Regarding the immune landscape in LV-Mets tissues, both TDX and TDX+ αPD1 combination display similar levels of CL Caspase-1 (Fig. 5d), an indication of pyroptosis induction by TDX. Moreover, mice treated with the combination achieves a high increase in CD8 + T cells and perforin densities, in LV-Mets sections, significantly higher than TDX than αPD1 or Vehicle-treated mice, which display the lowest levels (Fig. 5d). IFNγ was not secreted in LV-Mets tissues after the administration of single drugs or the combination (Fig. 5d), which contrast to the data observed in SC (Fig. 1d) and orthotopic primary tumor (Fig. 3c) MS-Mets tissues PRT-Mets that show high IFNγ levels.

Finally, we studied the antimetastatic effect and the molecular and cellular immune changes in lung metastases, within the same experiment and dosage described in detail in 3 (Fig. 3a), using the MSS mCRC model. In this case, the TDX+ αPD1combination eliminates LG-Mets since 71 % of mice are metastases-free in this organ at the end of the experiment; in contrast, the Vehicle-treated, TDX or αPD1 mice-treated groups showed micrometastases in all mice (Fig. 6a, b); whereas in the TDX+ αPD1-treated group all mice are free of micro-metastases in the LG, except for two mice that bear only one micrometastasis (Fig. 6c).

On the other hand, mice administered with TDX or αPD1 had a reduced number of metastases, as compared to Vehicle, but they did not generate enough anticancer activity on the treated mice to become metastases-free (Fig. 6a). Moreover, the 29 % of mice not eliminated by the combination (thus, bearing LG-Mets) still achieves a reduction in foci number as compared to single TDX or αPD1-treated, which reached in turn an antimetastatic effect higher than Vehicle-treated (Fig. 6c). Unfortunately, we could not study the molecular changes in LG-Mets tissues because of the low availability of micrometastatic foci and a high background immunohistochemical staining found in these tissues.

In summary, the potency of the antimetastatic or antitumor response induced by the TDX+ αPD1 combination is organ dependent. Moreover, we found distinct patterns of molecular and cellular immune activation in LV-Mets, LG-Mets, MS-Mets, PRT-Mets and subcutaneous or primary tumors, likely to be related with their mechanism of action and the potency of their anticancer effect.

### 3.6. TDX+ αPD1 combination induces potent antimetastic effect without systemic toxicity

At the end of the treatment with TDX (n = 9), αPD-1 (n = 8), TDX+ αPD1 (n = 6) or Vehicle (n = 6) in the immunocompetent SC CXCR4 + CT26 MSS CRC, applying the dosage described in detail in Fig. 3a, that reaches high anticancer activity, we analyzed mouse plasma and blood for its possible association with systemic toxicity.

Thus, we measured markers of renal and hepatic function which can detect toxicity in these organs, as well as markers of alteration in the blood cell linage. The assessment of hepatic transaminases (aspartate transaminase (AST) and alanine transaminase (ALT) in plasma, shows a normal hepatic function, since the TDX, αPD-1 or TDX+ αPD1-treated mice reach levels not significantly different from Vehicle-treated mice (Fig. 7a). Moreover, albumin, creatinine, and uric acid levels, determined in plasma, shows no statistical differences between TDX, αPD1 or the TDX+ αPD1-treated mice compared with Vehicle-treated mice, which indicates a lack of alteration in renal function associated with these treatments (Fig. 7a).

For its part, the study of the cell blood linage, including white blood cells (WBC) and red blood cells (RBC), hemoglobin (HGB) concentration, hematocrit (HCT), platelets (PLT) count, and procalcitonin (PCT) concentration shows normal levels in all parameters; thus, they are similar to those achieved in the Vehicle-treated mice, indicating a lack of toxicity in the cell blood lineage (Fig. 7b). Moreover, regarding WBC,

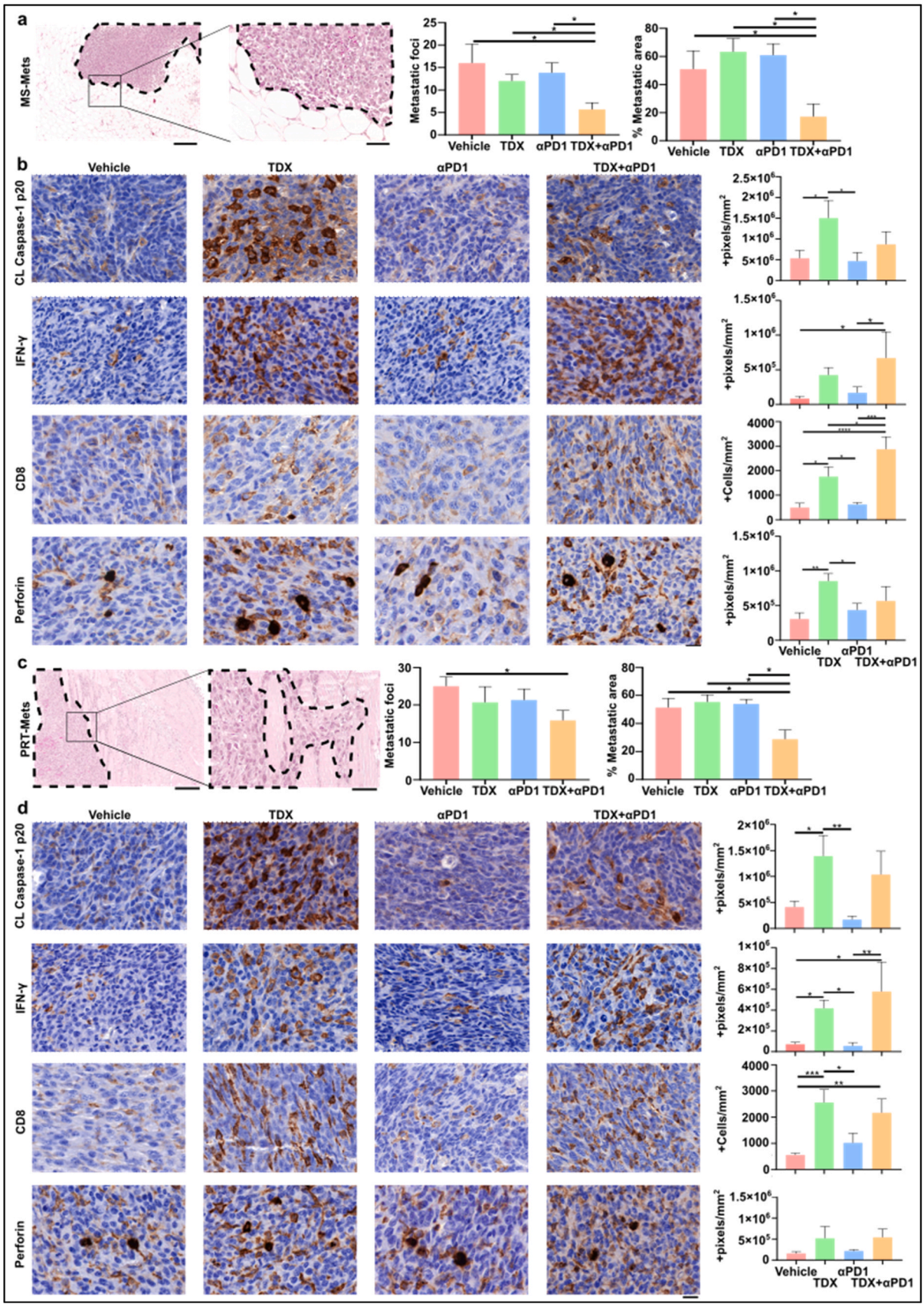


(caption on next page)

**Fig. 4.** TDX+ αPD1 combination therapy significantly reduces the metastatic burden in the mesentery and peritoneum in the orthotopic model (ORT MSS model). (a) Representative image of mesenteric metastatic foci (MS-Mets). Scale bars = 200 μm and 50 μm (zoom-in) and the quantitation of total metastatic foci per section and percentage of metastatic area per section in the mesentery. (b) Representative sample images of metastatic foci in the mesentery from mice treated with Vehicle, TDX, αPD1, or TDX+ αPD1 stained by IHC for CL Caspase-1, IFNγ, CD8 and perforin secretion. Measurement of CD8 positive cells or perforin positive pixels per $mm^2$ in the mesenteric tissue. Scale bars = 20 μm. (c) Illustrative image of peritoneal metastatic foci (PRT-Mets). Scale bars = 200 μm and 50 μm (zoom-in), and assessment of total metastatic foci per section and percentage of metastatic area per section in the peritoneum. (d) Representative images of metastatic foci in the peritoneum from mice of each experimental group stained by IHC for CL Caspase-1, IFNγ, CD8 and perforin. We calculate CD8 positive cells or positive pixels per $mm^2$ in the peritoneum. Scale bars = 20 μm. Error bars indicate ±SEM. * $p < 0.05$; ** $p < 0.01$; *** $p < 0.001$; **** $p < 0.0001$.

mice treated with TDX or TDX+ αPD1 groups display a total count and percent of neutrophils, lymphocytes, monocytes, eosinophils and basophils, similar to the vehicle-treated mice, therefore, exhibiting no toxicities related to treatment in the white cell linage lineage (Fig. 7c). Besides, mice in all groups do not show any signs of discomfort or weight loss during treatment, a task measured twice per week, throughout the experiment (Fig. 7d). In summary, the sequential TDX+ αPD1 dosage that obtains a potent antimetastatic activity does not induce toxicity based on the absence of alterations in hepatic and renal function, along with lack of changes in the RBC and WBC lineages and the lack of signs of disease or changes in mouse body weight, which indicates the absence of toxicity associated to the dosage applied in the TDX, αPD-1, or TDX+ αPD1 combination therapies.

## 4. Discussion

We found that treatment with the TDX nanotoxin, in immunocompetent CXCR4 + CT26 microsatellite stable (MSS) subcutaneous (sCRC) and metastatic CRC (mCRC) models is able to induce *in situ* pyroptosis mediated by the activation of NLRP3, Caspase-1, GSDMD and IL-1β to recruit and activate T cells in all tested cancer tissues, turning 'cold' into 'hot' cancer to achieve a potent antimetastatic and antitumor effect, without systemic toxicity. Our previous results obtained in immunosuppressed subcutaneous or metastatic CXCR4 + CRC or head and neck carcinoma cancer models induced pyroptosis but did not activate T cells because these mice lack T lymphocytes [3,8,11].

Moreover, the subsequent therapy of the FDA-approved inhibitor of the immune checkpoint αPD1, after TDX administration, further increases the T cell activation induced by TDX to unlock a remarkably synergistic antimetastatic effect to the anticancer effect. Followed, we described the distinct features of TDX and of the TDX+ αPD1 combination immunotherapy.

### *4.1. TDX nanotoxin-mediated pyroptosis recruits and activates CD8 T cells to induce immunogenic cell death and anticancer effect*

TDX achieves a highly selective delivery of the diphtheria toxin only in target tumor and metastases cells. Thus, TDX is a 90 nm structured nanoparticle, composed of monomers of 7 nm diameter. The about 12-fold higher diameter in the TDX nanotoxin compared to the monomer ensures a multivalent display of T22 ligands that yields a selective binding to cancer cells that overexpress CXCR4 (CXCR4 +) receptors to release the exotoxin in their cytosol. These nanostructures, either nanotransporters or nanoconjugates, reach a 70–85 % distribution of about the injected dose in cancer tissues, whereas they do not internalize in normal cells, as described [3,27,28]

Subsequently to the selective delivery of the diphtheria toxin by TDX in CXCR4 + LMet2 cancer cells activate pyroptosis mediated by Caspase-1 and GSDMD in vitro (Supplemental Fig. 1d), whereas in vivo TDX activates *in situ* pyroptosis in primary tumor tissues in ortotopic models derived from both CT26.mCXCR4 cell line and LMets2 cell line. This pyroptsois is mediated by the activation of NLRP3, Caspase-1 ansd IL-1β (Fig. 1e and Fig. 2c) [29]. Moreover, as a consequence of the induction of pyroptosis, we observed the recruitment of CD8 cells in scCRC tumors (Fig. 1) or orthotopic primary tumors (Fig. 2) and metastastatic tissues (Fig. 3, Fig. 4, Fig. 5) to secrete inflammatory cytokines that recruit CD8 T cells in both tumor and metastatic tissues, replicating the pyroptosis that we reported in immunosuppresed CXCR4 + CRC such as IL-1β or INFγ models, which however lack T cells [8,10,11]. Therefore, according to the induction of pyroptosis, we observed the secretion of the pro-inflammatory cytokine IFNγ or IL-1β in scCRC tumors and orthotopic tumors and also in MS-Mets and PRT-Mets associated with the recruitment of CD8 T cells according to previous reports indicating that IFNγ and IL-1β activates T cell migrationrecruitment and activation [30,31,32–34].

Next, in the 'hot' tumors, the release of cytotoxic proteins that T cells secrete to indude Immunogenic cell death of cancer cells and anticancer response, for instance in scCRC tumor size associated T cell activation and killing of target cancer cells, as determined by DNA condensation and T cell perforin secretion (Fig. 1c,e); and similarly, the primary tumor in the orthotopic tumor increae DNA condensation, associated with activation of CD8 T cells with perforin secretion (Fig. 3c).

Nevertheless, perforin is not the only cytotoxic protein that induces ICD. In this regard, the significant reduction of the metastatic number and area of burden in MS-Mets and PRT-Mets (Fig. 4) or LV-Mets (Fig. 5) associated with the activation of CD8 T cells; however, without perforin secretion; therefore, in these tissues, alternative cytotoxic proteins could release by the CD8 T cells. Thus, the observed cell killing and anticancer effect is likely to be mediated by immunogenic cell death (ICD) since the activated CD8 T cells release cytotoxic proteins, mediated either by perforin or granzymes) to induce ICD [26].

### *4.2. TDX sensitizes to αPD1 to achieve a remarkably synergistic effect in liver metastases when administered as the TDX+ αPD1 sequential combination therapy*

The αPD1 ICI therapy, as a single drug, in the CXCR4 mCRC MSS model, shows a lack of reduction in the number of mice LV-Mets free (Fig. 5a,b), a fact consistent with a similar lack of effect in MSS CRC in patients with LV-Mets when treated with αPD1 [17,17,22].

In huge contrast, when CRC MSS with LV-Mets treated with the TDX+ αPD1 combination, the after the administration of the second drug, αPD1, we found a synergistic response in LV-Mets, that ablates metastases in this organ since 86 % of the treated mice were cleared metastases. Remarkably, this effect associates with a high increase in CD8 + T cell recruitment and perforin secretion by T cells whereas single TDX or αPD1 treatment with found no recruitment of CD8 T cells nor secretion of perforin in LV-Mets (Fig. 5b).

Thus, single TDX or αPD1, as single drugs. maintain the immunosuppressive microenvironment, and immune tolerance of the non-pathological liver [35−37]; however, the TDX+ αPD1 therapeutic strategy overcomes LV immunosuppression by further activation of T cells that induces perforin secretion to induce IDC in target cancer cells. In contrast to our approach, the αPD1 + αCTLA-4 combination immunotherapy evaluated by other authors, using the same CT26 MSS mCRC model as in our experimental work, was ineffective in controlling LV-Mets [38].

In summary, to our knowledge, this is the first report on the LV-Mets ablation the TDX+ αPD1 combination immunotherapy, in MSS CRC models with LV-Mets, which suggests that the immunosuppressed ('cold') liver-bearing metastases could be manipulated to engage the T cells to induce ICD of metastases, overcoming the resistance of MSS metastases in this organ.

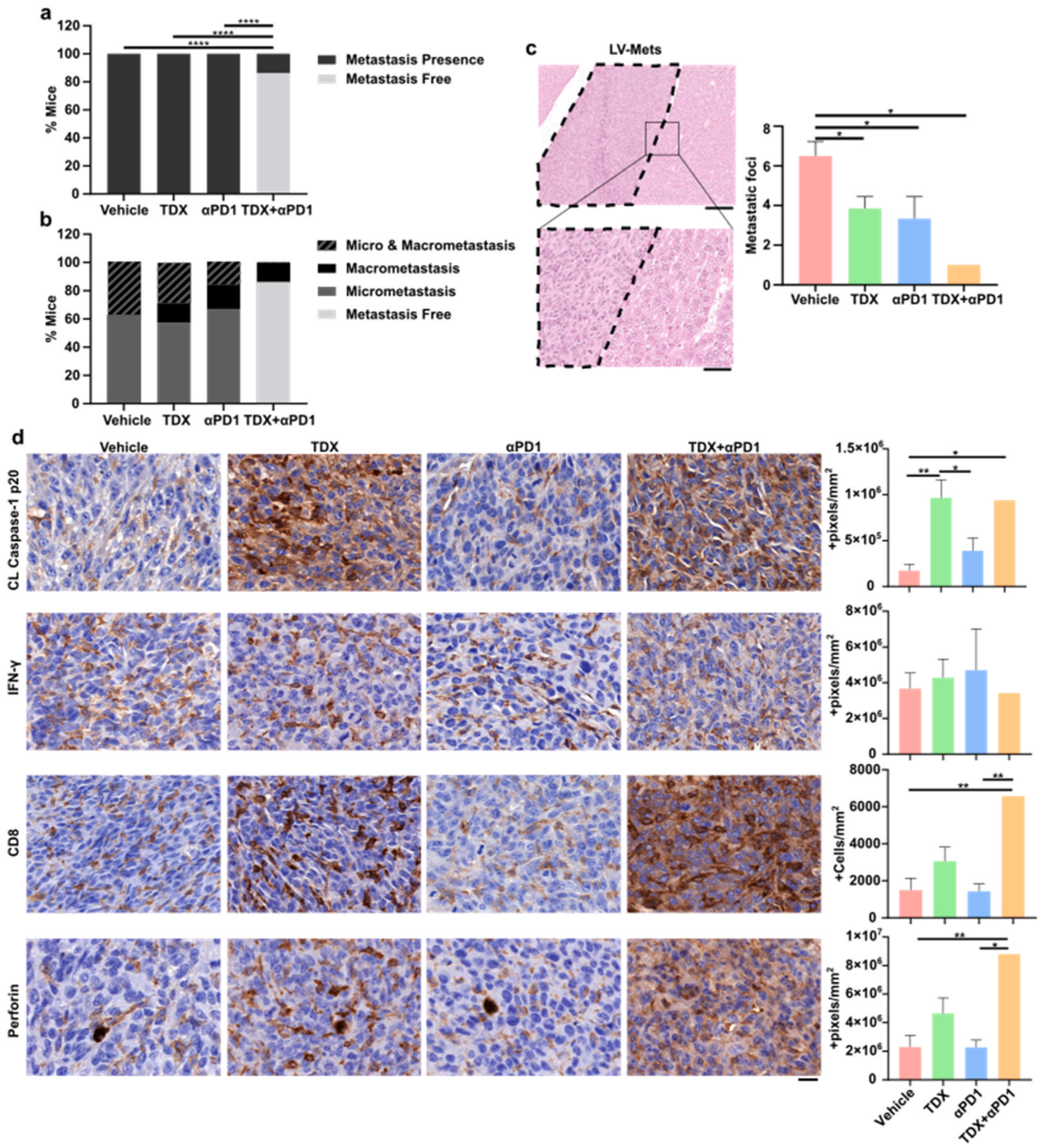


**Fig. 5.** TDX+ αPD1 combination therapy ablates liver metastases in the microsatellite-stable orthotopic mouse model (MSS ORT model). (a) Percentage of mice with presence of metastases or metastasis-free per group in the liver after treatment (b) Fraction of mice presenting macro-metastases, micrometastases, macro- and micrometastases or metastases free in the liver (c) Representative image of metastatic foci in the liver (LV-Mets) and the quantitation of total metastatic foci per section in the liver of mice with metastases per group. Scale bars = 200 μm and 50 μm (zoom in). (d) Illustrative images of metastatic foci in the liver from mice treated with Vehicle, TDX, αPD1, or TDX+ αPD1 combination therapy stained by IHC for CL casp-1, IFNγ, CD8 and perforin. Evaluation of positive stained pixels (CL caspase-1, IFNγ, perforin) or cells (CD8) per $mm^2$. Scale bars = 20 μm. Error bars indicate ±SEM. * $p < 0.05$; ** $p < 0.01$; **** $p < 0.0001$.

### *4.3. TDX sensitizes to αPD1 achieving tissue-specific responses, CD8 T cell recruitment, and secretion of cytokine or cytotoxic proteins in tumors and MS-Mets, PRT-Mets and LG-Mets*

Besides the specific pattern of T cell recruitment and activation and the cytotoxic protein secretion, associated with a synergistic LV-Mets response by the TDX+ αPD1 therapy, we also observed organ-specific patterns of anticancer cancer response associated with immune engagement.

Thus, in the scCRC tumor model, the TDX+ αPD1 induces a

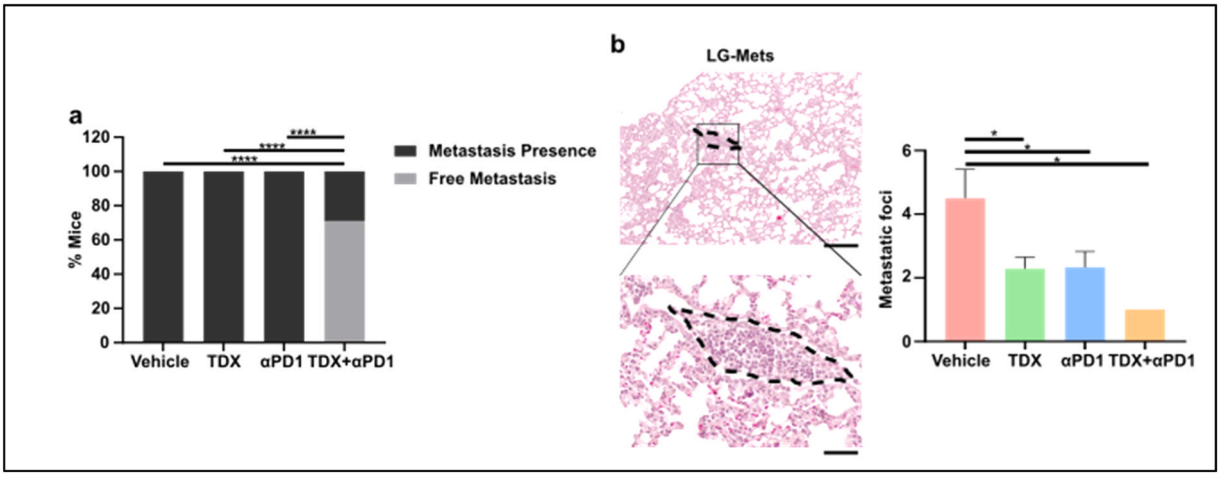


**Fig. 6.** TDX+ αPD1 combination therapy heals lung metastases in the microsatellite-stable orthotopic mouse model (MSS ORT model). (a) Proportion of mice per group with presence of metastases or metastasis-free in the lung per group, after treatment. (b) Sample image of metastatic foci in the lung (LG-Mets) and (c) Quantitation of total metastatic foci per section in the lung of mice with metastases. Scale bars = 200 μm and 50 μm (zoom in). Error bars indicate ±SEM. * $p < 0.05$; **** $p < 0.0001$.

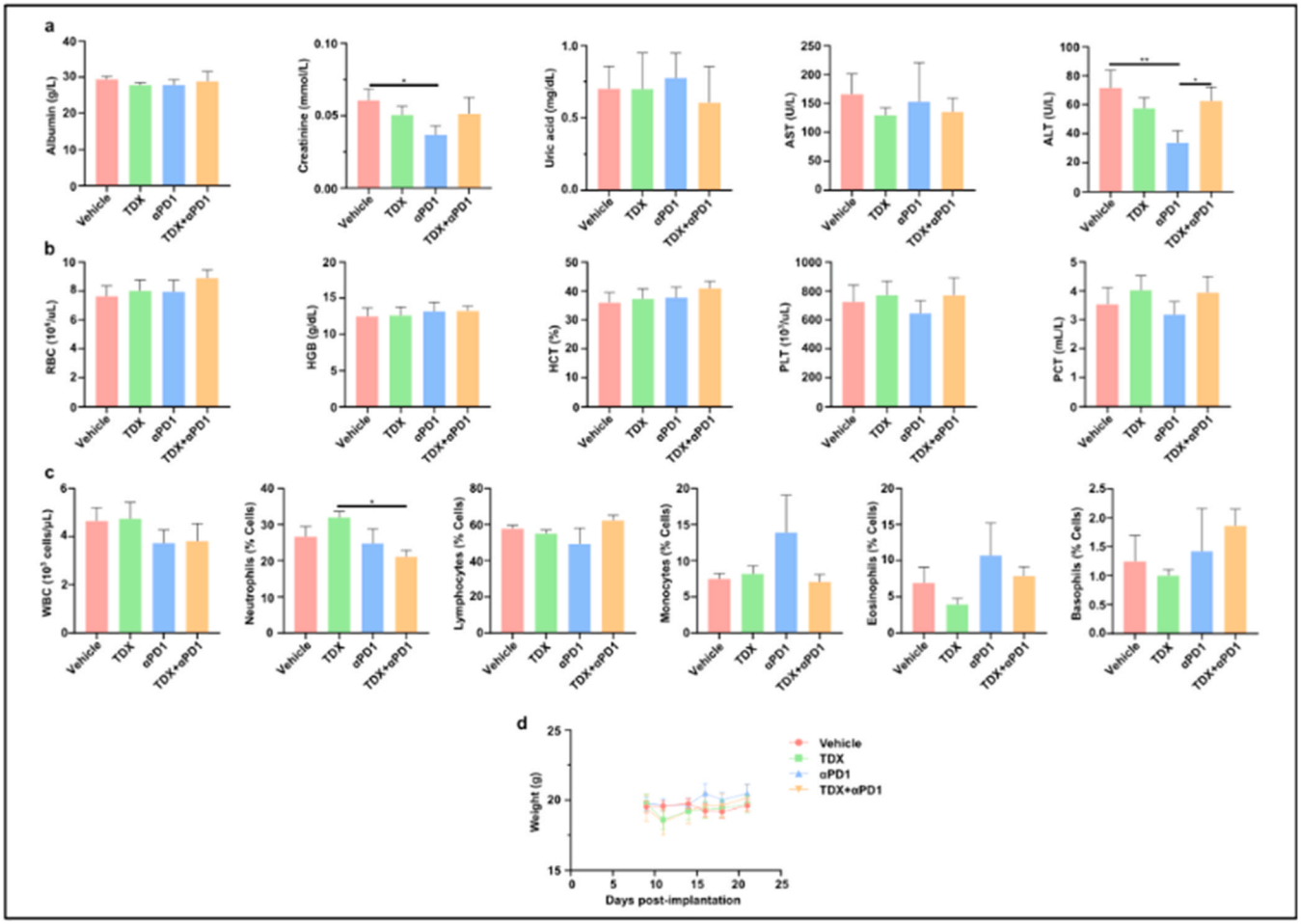


**Fig. 7.** Off-target toxicity of single drugs and NanoTDX+aPD1 combination therapy in the SC MSS CRC immunocompetent mice. (a) Quantitation of albumin, creatinine, uric acid, aspartate aminotransferase (AST) and alanine aminotransferase (ALT) in plasma. (b) Assessment of red blood cells (RBC), hemoglobin (HGB), hematocrit (HCT), platelets (PLT) and procalcitonin (PCT) counts in blood. (c) Analysis of total white blood cells (WBC) and percentage of neutrophils, lymphocytes, monocytes, eosinophils and basophils in blood. (d) Evolution of mouse body weight in each group during the in vivo subcutaneous experiment. Error bars indicate ±SEM. * $p < 0.05$; ** $p < 0.01$.

significant reduction of tumor growth, entering into negative growth (Fig. 1b) associated with further increases in IFNγ, CD8 + cell recruitment, perforin secretion, and an increase of DNA condensation, as compared to single TDX therapy (Fig. 1d).

Moreover, in the primary tumor of the orthotopic mCRC model, we observed a synergistic effect by the TDX+ αPD1 combination (Fig. 3b), associated with an increase in INFγ, high CD8, high perforin, and an increase in DNA condensation, as compared to no response by αPD1 therapy as a single drug (Fig. 3c).

We observed no perforin in MS-Mets and PRT-Mets, after TDX+ αPD1 treatment, despite finding a potent reduction in the number and area of metastases (Fig. 4a and Fig. 4c). Nevertheless, at the end of treatment, all mice bore metastases, which is a finding that is contrasts with the data on LV-free mice free after TDX+ αPD1 therapy (Fig. 5a,b, c). In MS-Mets and PRT-Mets the effect of the combination is associated with an increase in INFγ secretion and CD8 T cell recruitment, but no increase in perforin (Fig. 4b, Fig. 4d) as compared to αPD1 as a single drug, which induces no response and lacks INFg, CD8 T cells, or perforin.

Thus, it is likely that the potent control of metastases observed by the combination in MS-Mets and PRT-Mets was associated with the secretion of still unknown cytotoxic proteins alternative to perforin by T cells, such as Granzyme B or Granzyme A, that kill cancer cells, independently of perforin, as described [39,40]). This agrees with the ICD being mediated by the release of perforin cytotoxic granules once the immune synapse is established [26].

Interestingly, TDX+ αPD1 also reaches a synergistic effect in LG-Mets reaching 71 % of treated mice becoming LG-Mets-free, as compared to TDX or αPD1 as single drugs (Fig. 6). However, we could not study the immune mediators in this site because of the low availability of micrometastatic foci to study the mechanism of action that is associated with the ablation of LG-Mets by the combination.

The obtained data in our preclinical model may be dependent on the context-dependent immunoregulation and the strength response of metastases in different organs when treated with ICIs in the clinical setting [41].

### 4.4. Toxicity associated to TDX+ αPD1

Importantly, all the previous data on TDX or TDX+ αPD1 combination using the immunocompetent CXCR4 + CT26 MSS CRC models treated with the which induce a potent antitumor and antimetastatic effect, associates with a lack of toxicity in normal tissues, according with previous reports which avoiding the delivery of the exotoxin to non-tumor cells, Thus, we found absence of alterations in hepatic and renal function and normal levels in the white and red cell counts (Fig. 7).

Moreover, the lack of signs of disease, changes in mice, or changes in body weight supports the absence of toxicity, findings similar to the previous lack of systemic toxicity in immunosuppressed mouse models of animals of CRC [8], HNSCC [10,11] or lymphoma [42,43]). Consistently, our recent article devoted to evaluate the toxicity of repeated administration of TDX in the same CT26.mCXCR4 + model we observed lack of on-target and off-target toxicity [44]

Thus, they are overcoming some of the barriers that prevent the translation of the nanomedicines to patients, such as the targeted drug delivery in vivo because of the protein nature of TDX [45].

### 4.5. Immunotherapy in clinical trials for MSS mCRC

As said, a vast majority of CRC patients bearing mCRC with MSS do not respond to ICIs as single drugs [17,22,46]. Recently, clinical trials are being performed using combinations of approved ICI drugs [47,48]); however, so far αPD1 + αCTL-4 combinations in CRC patients did achieve responses on patients bearing non-liver metastases; however, those with LV-Mets have a poorer prognosis [47,49,50]. This agrees with LV-Mets treatment with classical chemotherapy and targeted therapies by developing resistance, conferring poor prognosis, and being the major cause of death in CRC patients [51,52]. On this basis, researchers propose to improve the prognosis and survival in CRC patients by developing novel therapies that target metastatic cells, especially LV-Mets, to overcome their resistance [53,54].

Moreover, still far from the clinical translation, the data obtained in our preclinical models achieving a potent antimetastatic response in the liver by administering the novel TDX+ αPD1 therapy provides useful insights in the development of effective immunotherapy combinations that could help reverse the resistance of LV-Mets to ICIs in CRC metastases observed in the patients, to turn them sensitive to αPD1 in CXCR4 + MSS mCRC.

### 4.6. Suggested mechanism of sensitization by TDX to the ICI αPD1 that mimicks the response to infection by diphtheria

The mechanism of action that underlies the cancer response obtained by TDX mimics the host response to diphtheria infection in epithelial cells, which inhibits eEF2 to induce ribotoxic stress, which activates the inflammasome to trigger pyroptosis to recruit and activate T cells to fight the infection [12,16,20,55,56].

Thus, the TDX-targeted drug delivery releases the diphtheria toxin in CXCR4 + epithelial cancer cells to inhibit eEF2 which may induce ribotoxic stress that activates the inflammasome to induce *in situ* pyroptosis mediated by Caspase-1 and GSDMD, which we have observed in all inflamed tumors and metastatic tissues (Fig. 1d; Fig. 2c; Fig. 3c; Fig. 4b, d; Fig. 5d).

Next, it is likely that the *in situ* pyroptotic induction, by TDX releases, large amount of neoantigens to trigger a secretion pattern of pro-inflammatory cytokines that reprograms the local TME to overcome the immune desert phenotype, changing the poor immune cells in all target cancer tissues by recruitment of T cells in MSS CRC [2,34], to achieve the objective of turning 'cold' to 'hot' tissues [57–59]. Thus, being pyroptosis highly immunogenic [6], it is likely that TDX is able to inactivate DNA repair systems, to generate a large amount of neoantigens, as described [15,38]) which are processed by antigen-presenting cells to locally recruit T cells in inflamed tissues to form antigen-specific cytotoxic T cells, which subsequently release cytotoxic proteins, such as perforin or granzymes, to induce ICD [58].

On this basis, we suggest that TDX converts target cancer tissue from 'cold' to 'hot' by recruiting T cells, and therefore, sensitizes to αPD1 when blocking this immune checkpoint in the preclinical MSS mCRC model to unleash a synergistic response greater by cytotoxic protein higher ICD as compared to that achieved by αPD1, as a single drug, which is resistant to αPD1 therapy. Remarkably, in LV-Mets (Fig. 5) the recruitt of T cells associates with a moderate effect; however, it does not induce in perforin by TDX, but contrarily the TDX+ αPD1 combination induces perforin secretion associated to a ablation of LV-Mets in most mice.

So far, MSS CRC patients are refractory to ICIs, likely due to incapacity to generate neoantigens; thus, they display low immunogenicity and an inability to recruit and activate T cells [17,22].

Our data yields insights into the development of innovative immunotherapy combinations that could improve their current low efficacy. Future studies are needed to understand the underlying mechanism of action in this TDX+ αPD1 combination inducing a response in tumor and metastatic tissues. Therefore, it is likely that our, or similar, approaches could overcome the resistance to ICIs in CRC patients with MSS. A limitation to the generalisability of the study is that it did not consider gender/sex issues.

## 5. Conclusions

The targeted TDX nanotoxin is able to induce *in situ* pyroptosis mediated by NLRP-3, Caspase-1, GSDMD and IL-1β and immunogenic cell death that recruit and activate T cells in all cancer tissues to achieve an antimetastatic and antitumor effect, in immunocompetent

CXCR4 + CT26 MSS sCRC and mCRC models without systemic toxicity. Moreover, the pyroptosis by TDX is also able to sensitize the inhibitor of checkpoint immune αPD1 to unleash a further increase of T cell activation to achieve a synergistic response greater by cytotoxic protein higher ICD, in contrast with the αPD1, as a single drug, which does not induce a response. Importantly, the TDX+ αPD1 ablates LV-Mets, suggesting that the immunosuppressed ('cold') liver-bearing metastases are able to overcome the resistance of MSS metastases, especially in this organ. Therefore, our novel immunotherapy approach, could give insights in targeted drug delivery to activate *in situ* pyroptosis, which, when combined with the ICIs will yield a synergistic effect, which in the near future could translate to the clinic to the benefit of a large majority of patients that bear MSS mCRC.

## CRediT authorship contribution statement

**Ugutz Unzueta:** Writing – review & editing, Funding acquisition. **Esther Vázquez:** Writing – review & editing, Validation, Funding acquisition. **Lorena Alba-Castellon:** Writing – review & editing, Writing – original draft, Visualization, Validation, Supervision, Project administration, Methodology, Funding acquisition, Conceptualization. **Isolda Casanova:** Writing – review & editing, Writing – original draft, Methodology. **Patricia Álamo:** Writing – review & editing, Methodology, Investigation. **Ramon Mangues:** Writing – review & editing, Writing – original draft, Visualization, Validation, Supervision, Project administration, Methodology, Funding acquisition, Conceptualization. **Luis M. Carrasco-Díaz:** Writing – review & editing, Writing – original draft, Methodology, Investigation. **Anna C. Virgili:** Writing – review & editing, Validation, Methodology. **Alberto Gallardo:** Writing – review & editing, Methodology. **Eric Voltà-Durán:** Writing – review & editing, Investigation. **David Páez:** Writing – review & editing, Validation, Methodology. **Antonio Villaverde:** Writing – review & editing, Validation, Funding acquisition. **Marc Otero-Mateo:** Investigation, Methodology, Writing – review & editing.

## Ethics approval and consent to participate

All experiments complied with the WMA Statement on animal use in biomedical research and/or the and EU recommendations (Directive 2010/63/EU) for experimental design and analysis in pharmacology care). Moreover, the experimental procedures were previously approved by the institutional Hospital de la Santa Creu i Sant Pau Animal Ethics Committee and the Catalonian Government, protocol nº 12001.

## Consent for publication

All authors have seen and approved the submission of their manuscript. We all consent the publication of this article in the open access *JITC* under the Creative Commons licence (CC BY- NC or CC-BY) to facilitate reuse of the content and authors retain copyright.

## Funding

This work was supported by Instituto de Salud Carlos III, Spain (ISCIII, co-funded by European Regional Development Fund (ERDF, a way to make Europe) for the projects PI24/01476 (RM, LAC, DP, ACV); PI21/00150 (RM, LAC, PA, ACV); PI20/00400 (UU, LAC, AG) PI24/00012, (IC) and PI23/00318 Grants (UU, LAC, AG, ACV). It was also funded by ISCIII (co-funded by European Social Fund (ESF investing in your future) through the FI19/00148 Pre-doctoral fellowship (LCD); CP19/00028 (UU) Contract Miguel Servet Fellowship and CP24/00111 (LAC) Contract Miguel Servet Fellowship. Josep Carreras Leukemia Research Institute financed a P/AG Grant to I.C. The Agencia Estatal de Investigacion (AEI) and Ministerio de Ciencia e Innovación, Sapin (MICINN) and Fondo Europeo de Desarrollo Regional (FEDER) supported the projects PID2020- 116174RB-I00 (AV); PID2019–105416RB-I00.AEI.10.13039/501100011033 (AV, EVD); PDC2022–133858-I00 (EV, EVD); PID2022–1368450.OB-10/AEI/10.13039/501100011033 (AV, EV, EVD) and FPU18/04615 (EVD) MICINN Predoctoral fellowship, Spain. The European Union, got support to run the EU COST Action CA17140 and CA21135 (RM, PA,UU, IC, LAC). The CIBER-BBN holds the CB06/01/1031 Grant and 4NanoMets Project to R.M., and NANOSCAPE to U·U.); and Agencia de Gestió de Ajuts Universitari i de Recerca (AGAUR) and Research Centres of Catalonia (CERCA) 2017-SGR-865 (RM, UU, PA, UU, IC), and 2021-SGR-01140 (RM, UU, LCD, UU, IC, LAC). The CIBER-BBN holds the CB06/01/1014 grant and VENOM4-CANCER Project to A.V., and NANOREMOTE Project to E.V. and AGAUR 2017SGR-229 (AV, EV).

## Declaration of Competing Interest

The authors declare the following financial interests/personal relationships which may be considered as potential competing interests: The authors declare the following financial interests/personal relationships which may be considered as potential competing interests: The authors declare the following financial interests/personal relationships which may be considered as potential competing interests: E.V., R.M. and A.V. are co-founders of Nanoligent, a company devoted to develop anticancer drugs based on proteins. U.U., E.V., A.V., R.M. and I.C. are cited as inventors in a patent application (EP11382005.4) covering the therapeutic use of T22. All other authors report no conflicts of interest in this work.

## Acknowledgments

We thank Luis Carlos Navas his support in the in vivo experiments and immunohistochemistry work. Our gratitude for the researchers who performed the histological and toxicity studies in the CIBER-BBN Nanotoxicology Unit 18 (http://www.nanbiosis.es/portfolio/u18-nanotoxicology-unit/), ICTS-NANBIOSIS, (entry accesses 3633, 3861 and 3157). We also thank the researchers that worked in the Protein production that enrolled in the ICTS "NANBIOSIS", more specifically their partial support by the Protein Production Platform of CIBER-BBN/IBB (http://www.nanbiosis.es/unit/u1- protein-production-platform-ppp/).

## Appendix A. Supporting information

Supplementary data associated with this article can be found in the online version at doi:10.1016/j.phrs.2025.107982.

## Data availability

Data will be made available on request.

## References

[1] L. Wang, H. Xu, L. Weng, J. Sun, Y. Jin, C. Xiao, Activation of cancer immunotherapy by nanomedicine, Front Pharm. 13 (2022), https://doi.org/10.3389/fphar.2022.1041073.
[2] C. Sui, H. Wu, X. Li, Y. Wang, J. Wei, J. Yu, et al., Cancer immunotherapy and its facilitation by nanomedicine, Biomark. Res. 12 (2024) 77, https://doi.org/10.1186/s40364-024-00625-6.
[3] M.V. Céspedes, U. Unzueta, A. Aviñó, A. Gallardo, P. Álamo, R. Sala, et al., Selective depletion of metastatic stem cells as therapy for human colorectal cancer, EMBO Mol. Med. 10 (2018), https://doi.org/10.15252/emmm.201708772.
[4] A. Falgàs, V. Pallarès, U. Unzueta, Y. Núñez, J. Sierra, A. Gallardo, et al., Specific cytotoxic effect of an auristatin nanoconjugate towards CXCR4+ diffuse large B-Cell lymphoma cells, Int. J. Nanomed. 16 (2021) 1869–1888, https://doi.org/10.2147/IJN.S289733.
[5] V. Pallarès, U. Unzueta, A. Falgàs, A. Aviñó, Y. Núñez, A. García-León, et al., A multivalent Ara-C-prodrug nanoconjugate achieves selective ablation of leukemic cells in an acute myeloid leukemia mouse model, Biomaterials 280 (2022) 121258, https://doi.org/10.1016/j.biomaterials.2021.121258.
[6] A.J. Legrand, M. Konstantinou, E.F. Goode, P. Meier, The diversification of cell death and immunity: memento mori, Mol. Cell 76 (2019) 232–242, https://doi.org/10.1016/j.molcel.2019.09.006.

[7] L. Sánchez-García, N. Serna, P. Álamo, R. Sala, M.V. Céspedes, M. Roldan, et al., Self-assembling toxin-based nanoparticles as self-delivered antitumoral drugs, J. Control. Release 274 (2018) 81–92, https://doi.org/10.1016/j.jconrel.2018.01.031.
[8] N. Serna, P. Álamo, P. Ramesh, D. Vinokurova, L. Sánchez-García, U. Unzueta, et al., Nanostructured toxins for the selective destruction of drug-resistant human CXCR4+ colorectal cancer stem cells, J. Control. Release 320 (2020) 96–104, https://doi.org/10.1016/j.jconrel.2020.01.019.
[9] R. Sala, E. Rioja-Blanco, N. Serna, L. Sánchez-García, P. Álamo, L. Alba-Castellón, et al., GSDMD-dependent pyroptotic induction by a multivalent CXCR4-targeted nanotoxin blocks colorectal cancer metastases, Drug Deliv. 29 (2022) 1384–1397, https://doi.org/10.1080/10717544.2022.2069302.
[10] E. Rioja-Blanco, I. Arroyo-Solera, P. Álamo, I. Casanova, A. Gallardo, U. Unzueta, et al., CXCR4-targeted nanotoxins induce GSDME-dependent pyroptosis in head and neck squamous cell carcinoma, J. Exp. Clin. Cancer Res. 41 (2022) 49, https://doi.org/10.1186/s13046-022-02267-8.
[11] E. Rioja-Blanco, A. Gallardo, I. Arroyo-Solera, P. Álamo, I. Casanova, U. Unzueta, et al., A novel CXCR4-Targeted diphtheria toxin nanoparticle inhibits invasion and metastatic dissemination in a head and neck squamous cell carcinoma mouse model, Pharmaceutics 14 (2022) 887, https://doi.org/10.3390/pharmaceutics14040887.
[12] K.S. Robinson, G.A. Toh, M.J. Firdaus, K.C. Tham, P. Rozario, C.K. Lim, et al., Diphtheria toxin activates ribotoxic stress and NLRP1 inflammasome-driven pyroptosis, J. Exp. Med. 220 (2023), https://doi.org/10.1084/jem.20230105.
[13] S. Tamaki, K. Suzuki, I. Abe, Y. Endo, N. Kakizawa, F. Watanabe, et al., Overexpression of satellite RNAs in heterochromatin induces chromosomal instability and reflects drug sensitivity in mouse cancer cells, Sci. Rep. 12 (2022) 10999, https://doi.org/10.1038/s41598-022-15071-3.
[14] J.C. Castle, M. Loewer, S. Boegel, J. de Graaf, C. Bender, A.D. Tadmor, et al., Immunomic, genomic and transcriptomic characterization of CT26 colorectal carcinoma, BMC Genom. 15 (2014) 190, https://doi.org/10.1186/1471-2164-15-190.
[15] G. Germano, S. Lamba, G. Rospo, L. Barault, A. Magrì, F. Maione, et al., Inactivation of DNA repair triggers neoantigen generation and impairs tumour growth, Nature 552 (2017) 116–120, https://doi.org/10.1038/nature24673.
[16] T. Bergsbaken, S.L. Fink, B.T. Cookson, Pyroptosis: host cell death and inflammation, Nat. Rev. Microbiol. 7 (2009) 99–109, https://doi.org/10.1038/nrmicro2070.
[17] Z. Zheng, T. Wieder, B. Mauerer, L. Schäfer, R. Kesselring, H. Braumüller, T cells in colorectal cancer: unravelling the function of different t cell subsets in the tumor microenvironment, Int. J. Mol. Sci. 24 (2023) 11673, https://doi.org/10.3390/ijms241411673.
[18] M.V. Céspedes, C. Espina, M.A. García-Cabezas, M. Trias, A. Boluda, M.T. Gómez del Pulgar, et al., Orthotopic microinjection of human colon cancer cells in nude mice induces tumor foci in all clinically relevant metastatic sites, Am. J. Pathol. 170 (2007) 1077–1085, https://doi.org/10.2353/ajpath.2007.060773.
[19] J. Folkman, Angiogenesis: initiation and modulation, Symp. Fundam. Cancer Res. 36 (1983) 201–208.
[20] S.-Y. Kwon, H. Thi-Thu Ngo, J. Son, Y. Hong, J.-J. Min, Exploiting bacteria for cancer immunotherapy, Nat. Rev. Clin. Oncol. 21 (2024) 569–589, https://doi.org/10.1038/s41571-024-00908-9.
[21] J. Yu, Q. Wang, X. Zhang, Z. Guo, X. Cui, Mechanisms of Neoantigen-Targeted induction of pyroptosis and ferroptosis: from basic research to clinical applications, Front Oncol. 11 (2021), https://doi.org/10.3389/fonc.2021.685377.
[22] K. Ganesh, Z.K. Stadler, A. Cercek, R.B. Mendelsohn, J. Shia, N.H. Segal, et al., Immunotherapy in colorectal cancer: rationale, challenges and potential, Nat. Rev. Gastroenterol. Hepatol. 16 (2019) 361–375, https://doi.org/10.1038/s41575-019-0126-x.
[23] P. Golstein, G.M. Griffiths, An early history of t cell-mediated cytotoxicity, Nat. Rev. Immunol. 18 (2018) 527–535, https://doi.org/10.1038/s41577-018-0009-3.
[24] E. Alspach, D.M. Lussier, R.D. Schreiber, Interferon γ and its important roles in promoting and inhibiting spontaneous and therapeutic cancer immunity, Cold Spring Harb. Perspect. Biol. 11 (2019) a028480, https://doi.org/10.1101/cshperspect.a028480.
[25] W.H. Fridman, L. Zitvogel, C. Sautès–Fridman, G. Kroemer, The immune contexture in cancer prognosis and treatment, Nat. Rev. Clin. Oncol. 14 (2017) 717–734, https://doi.org/10.1038/nrclinonc.2017.101.
[26] I. Voskoboinik, J.C. Whisstock, J.A. Trapani, Perforin and granzymes: function, dysfunction and human pathology, Nat. Rev. Immunol. 15 (2015) 388–400, https://doi.org/10.1038/nri3839.
[27] A. Villaverde, Unzueta, Céspedes, Ferrer-Miralles, Casanova, Cedano, et al., Intracellular CXCR4+ cell targeting with T22-empowered protein-only nanoparticles, Int. J. Nanomed. (2012) 4533, https://doi.org/10.2147/IJN.S34450.
[28] M.V. Céspedes, U. Unzueta, P. Álamo, A. Gallardo, R. Sala, I. Casanova, et al., Cancer-specific uptake of a liganded protein nanocarrier targeting aggressive CXCR4 + colorectal cancer models, Nanomedicine 12 (2016) 1987–1996, https://doi.org/10.1016/j.nano.2016.04.003.
[29] Z. Dai, W.-C. Liu, X.-Y. Chen, X. Wang, J.-L. Li, X. Zhang, Gasdermin D-mediated pyroptosis: mechanisms, diseases, and inhibitors, Front Immunol. 14 (2023), https://doi.org/10.3389/fimmu.2023.1178662.
[30] C. Nakajima, Y. Uekusa, M. Iwasaki, N. Yamaguchi, T. Mukai, P. Gao, et al., A role of interferon-gamma (IFN-gamma) in tumor immunity: t cells with the capacity to reject tumor cells are generated but fail to migrate to tumor sites in IFN-gamma-deficient mice, Cancer Res. 61 (2001) 3399–3405.
[31] L. Ni, J. Lu, Interferon gamma in cancer immunotherapy, Cancer Med. 7 (2018) 4509–4516, https://doi.org/10.1002/cam4.1700.
[32] F. Castro, A.P. Cardoso, R.M. Gonçalves, K. Serre, M.J. Oliveira, Interferon-Gamma at the crossroads of tumor immune surveillance or evasion, Front Immunol. 9 (2018), https://doi.org/10.3389/fimmu.2018.00847.
[33] B. Van Den Eeckhout, J. Tavernier, S. Gerlo, Interleukin-1 as innate mediator of t cell immunity, Front Immunol. 11 (2021), https://doi.org/10.3389/fimmu.2020.621931.
[34] C. Huang, J. Li, R. Wu, Y. Li, C. Zhang, Targeting pyroptosis for cancer immunotherapy: mechanistic insights and clinical perspectives, Mol. Cancer 24 (2025) 131, https://doi.org/10.1186/s12943-025-02344-4.
[35] D. Zeng, M. Wang, J. Wu, S. Lin, Z. Ye, R. Zhou, et al., Immunosuppressive microenvironment revealed by immune cell landscape in Pre-metastatic liver of colorectal cancer, Front Oncol. 11 (2021), https://doi.org/10.3389/fonc.2021.620688.
[36] N. Taniki, N. Nakamoto, P.-S. Chu, M. Ichikawa, T. Teratani, T. Kanai, Th17 cells in the liver: balancing autoimmunity and pathogen defense, Semin Immunopathol. 44 (2022) 509–526, https://doi.org/10.1007/s00281-022-00917-9.
[37] K. Wu, G. Zhang, C. Shen, L. Zhu, C. Yu, K. Sartorius, et al., Role of t cells in liver metastasis, Cell Death Dis. 15 (2024) 341, https://doi.org/10.1038/s41419-024-06726-2.
[38] W.W. Ho, I.L. Gomes-Santos, S. Aoki, M. Datta, K. Kawaguchi, N.P. Talele, et al., Dendritic cell paucity in mismatch repair–proficient colorectal cancer liver metastases limits immune checkpoint blockade efficacy, Proc. Natl. Acad. Sci. 118 (2021), https://doi.org/10.1073/pnas.2105323118.
[39] J.A. Trapani, M.J. Smyth, Functional significance of the perforin/granzyme cell death pathway, Nat. Rev. Immunol. 2 (2002) 735–747, https://doi.org/10.1038/nri911.
[40] R. Thompson, X. Cao, Reassessing granzyme B: unveiling perforin-independent versatility in immune responses and therapeutic potentials, Front Immunol. 15 (2024), https://doi.org/10.3389/fimmu.2024.1392535.
[41] W. Pao, C.-H. Ooi, F. Birzele, A. Ruefli-Brasse, M.A. Cannarile, B. Reis, et al., Tissue-Specific immunoregulation: a call for better understanding of the "Immunostat" in the context of cancer, Cancer Discov. 8 (2018) 395–402, https://doi.org/10.1158/2159-8290.CD-17-1320.
[42] A. Falgàs, A. Garcia-León, Y. Núñez, N. Serna, L. Sánchez-Garcia, U. Unzueta, et al., A diphtheria toxin-based nanoparticle achieves specific cytotoxic effect on CXCR4 + lymphoma cells without toxicity in immunocompromised and immunocompetent mice, Biomed. Pharmacother. 150 (2022) 112940, https://doi.org/10.1016/j.biopha.2022.112940.
[43] A. Falgàs, V. Pallarès, U. Unzueta, M.V. Céspedes, I. Arroyo-Solera, M.J. Moreno, et al., A CXCR4-targeted nanocarrier achieves highly selective tumor uptake in diffuse large B-cell lymphoma mouse models, Haematologica 105 (2020) 741–753, https://doi.org/10.3324/haematol.2018.211490.
[44] L. Carrasco-Díaz, A. Gallardo, E. Voltà-Durán, A. Virgili, D. Páez, A. Villaverde, et al., A targeted nanotoxin inhibits colorectal cancer growth through local tumor pyroptosis and eosinophil infiltration and degranulation, Int. J. Nanomed. 20 (2025) 2445–2460, https://doi.org/10.2147/IJN.S499192.
[45] P. Joyce, C.J. Allen, M.J. Alonso, M. Ashford, M.S. Bradbury, M. Germain, et al., A translational framework to DELIVER nanomedicines to the clinic, Nat. Nanotechnol. 19 (2024) 1597–1611, https://doi.org/10.1038/s41565-024-01754-7.
[46] Q. Lei, D. Wang, K. Sun, L. Wang, Y. Zhang, Resistance mechanisms of Anti-PD1/PDL1 therapy in solid tumors, Front Cell Dev. Biol. 8 (2020), https://doi.org/10.3389/fcell.2020.00672.
[47] E.X. Chen, J.M. Loree, E. Titmuss, D.J. Jonker, H.F. Kennecke, S. Berry, et al., Liver metastases and immune checkpoint inhibitor efficacy in patients with refractory metastatic colorectal cancer, JAMA Netw. Open 6 (2023) e2346094, https://doi.org/10.1001/jamanetworkopen.2023.46094.
[48] A.J. Bullock, B.L. Schlechter, M.G. Fakih, A.M. Tsimberidou, J.E. Grossman, M. S. Gordon, et al., Botensilimab plus balstilimab in relapsed/refractory microsatellite stable metastatic colorectal cancer: a phase 1 trial, Nat. Med. 30 (2024) 2558–2567, https://doi.org/10.1038/s41591-024-03083-7.
[49] B. Saberzadeh-Ardestani, J.C. Jones, J.M. Hubbard, R.R. McWilliams, T. R. Halfdanarson, Q. Shi, et al., Association between survival and metastatic site in mismatch Repair–Deficient metastatic colorectal cancer treated with First-line pembrolizumab, JAMA Netw. Open 6 (2023) e230400, https://doi.org/10.1001/jamanetworkopen.2023.0400.
[50] P.C. Tumeh, M.D. Hellmann, O. Hamid, K.K. Tsai, K.L. Loo, M.A. Gubens, et al., Liver metastasis and treatment outcome with Anti-PD-1 monoclonal antibody in patients with melanoma and NSCLC, Cancer Immunol. Res. 5 (2017) 417–424, https://doi.org/10.1158/2326-6066.CIR-16-0325.
[51] F.A. Zeineddine, M.A. Zeineddine, A. Yousef, Y. Gu, S. Chowdhury, A. Dasari, et al., Survival improvement for patients with metastatic colorectal cancer over twenty years, NPJ Precis. Oncol. 7 (2023) 16, https://doi.org/10.1038/s41698-023-00353-4.
[52] A.I. Valderrama-Treviño, B. Barrera-Mera, J.C. Ceballos-Villalva, E.E. Montalvo-Javé, Hepatic metastasis from colorectal cancer, Eur. J. Hepatogastroenterol 7 (2017) 166–175, https://doi.org/10.5005/jp-journals-10018-1241.
[53] S. Kopetz, G.J. Chang, M.J. Overman, C. Eng, D.J. Sargent, D.W. Larson, et al., Improved survival in metastatic colorectal cancer is associated with adoption of hepatic resection and improved chemotherapy, J. Clin. Oncol. 27 (2009) 3677–3683, https://doi.org/10.1200/JCO.2008.20.5278.
[54] G.G. Van den Eynden, A.W. Majeed, M. Illemann, P.B. Vermeulen, N.C. Bird, G. Høyer-Hansen, et al., The multifaceted role of the microenvironment in liver

metastasis: biology and clinical implications, Cancer Res. 73 (2013) 2031–2043, https://doi.org/10.1158/0008-5472.CAN-12-3931.
[55] M.B. Dwinell, N. Lügering, L. Eckmann, M.F. Kagnoff, Regulated production of interferon-inducible T-cell chemoattractants by human intestinal epithelial cells, Gastroenterology 120 (2001) 49–59, https://doi.org/10.1053/gast.2001.20914.
[56] J. Xu, G. Núñez, The NLRP3 inflammasome: activation and regulation, Trends Biochem. Sci. 48 (2023) 331–344, https://doi.org/10.1016/j.tibs.2022.10.002.
[57] R. Tang, J. Xu, B. Zhang, J. Liu, C. Liang, J. Hua, et al., Ferroptosis, necroptosis, and pyroptosis in anticancer immunity, J. Hematol. Oncol. 13 (2020) 110, https://doi.org/10.1186/s13045-020-00946-7.
[58] Y. Tan, Q. Chen, X. Li, Z. Zeng, W. Xiong, G. Li, et al., Pyroptosis: a new paradigm of cell death for fighting against cancer, J. Exp. Clin. Cancer Res. 40 (2021) 153, https://doi.org/10.1186/s13046-021-01959-x.
[59] S.S. Faria, A.J. Fernando, V.C.C. de Lima, A.G. Rossi, J.M.A. de Carvalho, K. G. Magalhães, Induction of pyroptotic cell death as a potential tool for cancer treatment, J. Inflamm. 19 (2022) 19, https://doi.org/10.1186/s12950-022-00316-9.